Inviscid Flowfield of an Unsteady Airfoil

W. J. McCroskey*
U.S. Army Air Mobility R & D Laboratory, Moffet Field, Calif.

Simple formulas have been developed from thin airfoil theory to describe the detailed inviscid, incompressible flowfield of an unsteady airfoil with thickness and camber. The solutions allow the various physical aspects of the problem and the parameters of the unsteady motion to be identified easily. The results agree well with numerical calculations and pressure measurements. The unsteady phase lag and attenuation of the inviscid pressure gradients near the leading edge explain the dynamic delay in laminar boundary-layer separation on oscillating airfoils, but not the characteristics of dynamic stall.

Nomenclature

A, a = pitch axis location relative to the leading edge and midchord, respectively, nondimensionalized by c and $c/2$
$C(k)$ = Theodorsen function, $F+iG$
$C^*(k, X)$ = modified Theodorsen function for velocity
C_p = pressure coefficient; $(p-p_\infty)/\frac{1}{2}\rho u_\infty{}^2$
C_{l_α} = steady lift curve slope
c = airfoil chord
F, F^* = real parts of C and C^*, respectively
f = real part of S
G, G^* = imaginary parts of C and C^*, respectively
g = imaginary part of S
h = plunging displacement
$I_w, I_w{}^*$ = integrals giving the effect of the wake on the pressure and velocity distributions, respectively
$J_n(k)$ = Bessel function of the first kind
k = reduced frequency, $\omega c/2u_\infty$
p = pressure
R = ratio of unsteady to steady solutions for pressure coefficient on a flat plate
Re = Reynolds number based on u_∞ and c
r_0 = leading-edge radius, nondimensionalized by c
S = ratio of unsteady to steady solutions for pressure gradients on a flat plate
s = dimensionless time, $2u_\infty t/c$
T = ratio of unsteady to steady solutions for velocity on a flat plate
t = time
U = surface velocity on the airfoil, nondimensionalized by u_∞
u_∞ = freestream velocity
V_t, V_c, V_a = thickness, camber, and angle-of-attack components of surface velocity on a steady airfoil
w_0 = vertical gust velocity, nondimensionalized by u_∞
X, x = chordwise coordinate measured from the leading and from midchord, respectively, nondimensionalized by c and $c/2$
$Y_n(k)$ = Bessel function of the second kind
α = instantaneous angle of attack relative to the "ideal" incidence
γ_w = wake vorticity, nondimensionalized by $c/2$ and u_∞
ξ = chordwise coordinate in the wake measured from midchord, nondimensionalized by $c/2$
ρ = density
$\Phi(s)$ = Wagner lift deficiency function
$\Phi^*(s, X)$ = modified Wagner function for velocity
ϕ = nondimensional velocity potential
$\Psi(s)$ = Kussner lift deficiency function
$\Psi^*(s, X)$ = modified Kussner function for velocity
ω = angular velocity

Presented as Paper 72-681 at the AIAA 5th Fluid and Plasma Dynamics Conference, Boston, Mass., June 26–28, 1972; submitted July 20, 1972; revision received March 12, 1973.

Index categories: Nonsteady Aerodynamics; Rotary Wing Aerodynamics; Jets, Wakes, and Viscid-Inviscid Interactions.

* Research Scientist, Ames Directorate. Associate Fellow AIAA.

I. Introduction

FOR many years, unsteady thin airfoil theory has been used to explain and predict aerodynamic and hydrodynamic flutter, airloads during rapid aircraft maneuvers or gust entry, and periodic fluid dynamic forces in turbomachinery. However, the important problem of dynamic stall is still not well understood. To begin to analyze this complex viscous-inviscid interaction problem, one needs more details of the inviscid flowfield structure and greater accuracy in the leading-edge region than are readily available from existing solutions.[1-10]

This paper does not attempt to solve the dynamic stall problem, but the first part of it contains simple and concise formulas that describe the detailed incompressible, inviscid flowfield of an unsteady airfoil with thickness and camber. Perhaps these solutions will be useful in future unsteady boundary-layer analyses. The second part of the paper considers the extent to which purely inviscid considerations can explain observed differences between static and dynamic airfoil behavior, particularly regarding laminar boundary-layer separation and the onset of dynamic stall.

II. Analysis

The twin goals of the analysis are simplicity and accuracy: simplicity to allow the parameters and physical effects of the unsteady motion to be identified easily, and sufficient accuracy to permit meaningful unsteady boundary-layer or viscous-inviscid interaction studies to proceed. In this section, we consider only the basic concepts of the analysis and cite the results. Further details are given in the Appendix.

The basic idea, illustrated in Fig. 1, is an extension of Allen's method[11-12] for steady airfoils; this method overcomes the difficulties and inaccuracies of classical linearized thin airfoil theory without losing its explicit simplicity. Consider a rigid airfoil executing unsteady pitching and plunging motion in an irrotational, incompressible fluid. As the bound circulation of the airfoil changes, vorticity is shed into a thin wake that trails behind. The velocity potential satisfies the Laplace equation, subject to the boundary condition of tangential flow along the surface of the airfoil and along the constant pressure sheet of trailing vorticity. Let us invoke a slight extension of the well-known mean surface approximation by applying this boundary condition along the entire X-axis, on the airfoil and in the wake as well, where the trailing vorticity is assumed to drift with velocity u_∞. Then this linearization permits us to write the velocity potential as a sum of separable thickness, camber, and angle-of-attack components, as follows:

$$\phi = \phi_t + \phi_c + \phi_a \tag{1}$$

The present analysis differs from previous investigations of unsteady airfoils with thickness[5-10] primarily in the way in which

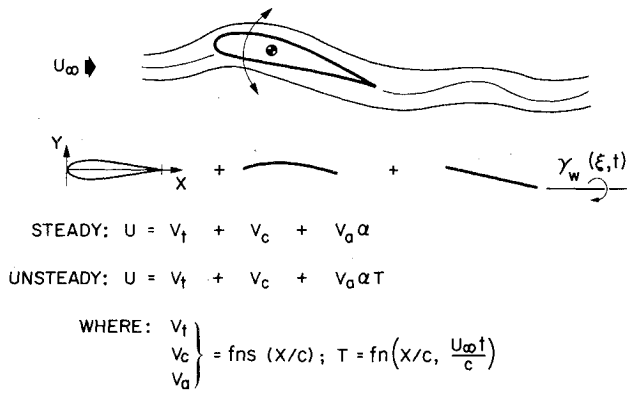

Fig. 1 The unsteady flow over an airfoil divided into thickness, camber, and angle-of-attack components. The functions V_t, V_c, and V_a are calculated from steady airfoil theory and T is the ratio of unsteady to steady velocity on a flat plate.

ϕ is calculated. First, we recognize that the thickness and camber solutions in Eq. (1) are independent of time for a rigid airfoil. Second, we note that the unsteady wake contributions to ϕ are the same as those for a flat plate; e.g., Theodorsen's solution[1] for oscillatory motion, Wagner's problem[2] of impulsive motion, or Kussner's or von Kármán and Sears' sharp-edged gusts.[3,4] Then as indicated in Fig. 1, the unsteady solution for the velocity along the surface of the airfoil is simply the sum of thickness, camber, and angle-of-attack components

$$U(X,t) = V_t \pm V_c \pm V_a \alpha T \tag{2}$$

where the signs refer to the upper and lower surfaces, respectively, and $\alpha(t)$ is in radians.† The function $T(X,t)$, which contains all the unsteady effects, is the ratio of the unsteady to quasi-steady solutions for a flat plate at angle of attack α. In other words, we have merely substituted αT in place of α in the steady theory to obtain an unsteady solution of comparable quality.

From the unsteady Bernouilli equation, the chordwise pressure distribution is

$$C_p = 1 - U^2 - (2c/u_\infty)\,\partial\phi_a/\partial t \tag{3}$$

where U is given by Eq. (2) and $\partial\phi_a/\partial t$ can be developed from the appropriate thin airfoil solution for an unsteady flat plate. Considerably more insight and simplicity can be achieved, however, if we evaluate U^2 in the classical manner of thin airfoil theory for small disturbances. For the upper surface, for example, Eq. (2) can be squared and rearranged as follows:

$$U^2 = 2(V_t + V_c + V_a\alpha T) - 1 + (V_t + V_c - 1)^2 + V_a^2\alpha^2 T^2 + 2(V_t + V_c - 1)V_a\alpha T$$
$$= 2(V_t + V_c + V_a\alpha T) - 1 + \text{second-order terms}$$

Therefore, the linearized pressure coefficient is

$$C_{p\,\mathrm{LIN}} = 2(1 - V_t - V_c - V_a\alpha T) - (2c/u_\infty)\,\partial\phi_a/\partial t$$

or

$$\tfrac{1}{2}C_{p\,\mathrm{LIN}} = 1 - V_t - V_c - V_a\alpha R \tag{4}$$

where $R = T + (c/u_\infty V_a\alpha)\,\partial\phi/\partial t$. The important point here is that $R(X,t)$ is directly analogous to $T(X,t)$, in that it contains all the unsteady effects for the pressure distribution, and it is the ratio of the unsteady to quasi-steady solutions for a flat plate at angle of attack α.

† For comparison with the notation of Ref. 12, $V_t = v/V$; $V_c = \Delta v/V$; $V_a = C_{l_\alpha}\Delta v_a/V$; $\alpha = (\alpha_g - \alpha_i)$; α_g is the instantaneous geometric incidence; and α_i is the "ideal" incidence, at which the steady-state stagnation point is located at the geometric leading edge. The details of the thickness and camber functions depend upon the airfoil geometry, but V_t always vanishes at the leading edge and rises to values of order 1 elsewhere, and for most airfoils $0 \leqq V_c < 0.5$. The function V_a attains values of order $(2/r_0)^{1/2}$ at the leading edge and $[(1-X)/X]^{1/2}$ downstream.

The location of the stagnation point can be determined in a manner analogous to van Dyke's[13] and Ville's[14] treatment of the leading-edge region of a steady airfoil. That is Eq. (2) is applied to an inclined parabola or ellipse with the same leading edge radius as the airfoil. The result in the present nomenclature is

$$V_t = \left(\frac{X}{X + r_0/2}\right)^{1/2}\left[1 + (2r_0)^{1/2} + \mathcal{O}(r_0)\right] \tag{5}$$

$$V_c + V_a\alpha T = \left(\frac{1}{X + r_0/2}\right)^{1/2}\left[1 + (2r_0)^{1/2} + \mathcal{O}(\alpha_i r_0^{1/2})\right]\alpha T \tag{6}$$

Therefore, to second order the stagnation point is located on the lower surface of the airfoil at the chordwise position

$$X_0 = \alpha^2 T^2(0,t) \tag{7}$$

Alternatively, R may be substituted for T in the leading-edge region, as shown in the next section.

The Functions T and R

We turn now to the two functions that describe the differences between static and dynamic behavior. Both R and T consist of "noncirculatory" and "circulatory" components; the former depend only upon the instantaneous motion of the airfoil, while the circulatory components depend upon the history of the motion through the influence of the time-dependent vorticity in the wake.

Almost every investigator of unsteady airfoils considers the linearized pressure distribution; the results of the analysis summarized in the Appendix are

$$\alpha R = QI_w - \frac{1}{4}\frac{\dot\alpha c}{u_\infty} + 2X\left[\frac{\dot\alpha c}{u_\infty} + \frac{\dot h c}{2u_\infty} + \frac{\ddot\alpha c^2}{4u_\infty^2}(X - \tfrac{1}{2} + 2A)\right] \tag{8}$$

where

$$Q(t) = \alpha + \frac{\dot h}{u_\infty} + \left(\frac{3}{4} - A\right)\frac{\dot\alpha c}{u_\infty}$$

i.e., Q is the instantaneous vertical velocity at the rear neutral point, $X = \frac{3}{4}$, and the wake effects are described by

$$I_w\left(\frac{u_\infty t}{c}\right) = \int_1^\infty \frac{\xi}{(\xi^2-1)^{1/2}}\gamma_w\,d\xi \Big/ \int_1^\infty \frac{\xi+1}{(\xi^2-1)^{1/2}}\gamma_w\,d\xi \tag{9}$$

For sinusoidal oscillations, $I_w = C(k)$, the Theodorsen function. Other fundamental special cases are 1) indicial response to a step change in α

$$\alpha R = \Delta\alpha\Phi(s) \qquad \text{(Wagner Function)}$$

2) Sharp-edged gust response

$$\alpha R = w_0\Psi(s) \qquad \text{(Kussner Function)}$$

Using these known results in Eq. (4), we can determine the unsteady pressure distribution on the airfoil and see explicitly the predominant effects of airfoil geometry and unsteady motion.

Unfortunately, the analogous expression for the velocity function

$$\alpha T = QI_w^* + (X - \tfrac{1}{4}\dot\alpha c/u_\infty) \tag{10}$$

cannot be expressed entirely in terms of known functions. Rather, the wake integrals depend upon X as well as $u_\infty t/c$; viz.,

$$I_w^*(u_\infty t/c, X) = \frac{\displaystyle\int_1^\infty \frac{\xi}{(\xi^2-1)^{1/2}}\gamma_w\,d\xi - 2X\int_1^\infty \frac{1}{(\xi+1-2X)(\xi^2-1)^{1/2}}\gamma_w\,d\xi}{\displaystyle\int_1^\infty \frac{\xi+1}{(\xi^2-1)^{1/2}}\gamma_w\,d\xi} \tag{11}$$

The denominator and the first term in the numerator of Eq. (11) are identical to the integrals in Eq. (9). It should be mentioned that these integrals present formal mathematical difficulties of convergence, but fortunately this has been treated exhaustively by previous authors,[1-4,15] and their analyses and results can be utilized directly. The second term in the numerator represents the wake contribution to $\partial\phi/\partial t$ in Eq. (3). It vanishes at the leading edge and is less singular than $1/(1-X)^{1/2}$ at the trailing

Table 1 Values of the modified Theodorsen function $C^* = F^* + iG^*$ for velocity

k	F^*				
	$X = 0$	$X = 0.25$	$X = 0.50$	$X = 0.75$	$X = 0.90$
0.025	0.9543	0.9518	0.9481	0.9412	0.9295
0.050	0.9090	0.9013	0.8901	0.8685	0.8317
0.100	0.8319	0.8115	0.7807	0.7203	0.6161
0.200	0.7275	0.6822	0.6112	0.4672	0.2146
0.300	0.6649	0.5994	0.4943	0.2755	−0.1147
0.500	0.5979	0.5044	0.3488	0.0111	−0.6088
1.000	0.5394	0.4117	0.1864	−0.3390	−1.3625
2.000	0.5129	0.3626	0.0821	−0.6291	−2.1406
5.000	0.5023	0.3394	0.0203	−0.8724	−3.0625
10.000	0.5006	0.3349	0.0058	−0.9558	−3.5572
			$-G^*$		
0.025	0.0872	0.1010	0.1234	0.1717	0.2632
0.050	0.1306	0.1557	0.1968	0.2866	0.4584
0.100	0.1723	0.2135	0.2828	0.4380	0.7406
0.200	0.1886	0.2463	0.3477	0.5857	1.0672
0.300	0.1793	0.2432	0.3596	0.6445	1.2415
0.500	0.1507	0.2158	0.3415	0.6721	1.4101
1.000	0.1002	0.1552	0.2727	0.6258	1.5211
2.000	0.0576	0.0955	0.1861	0.5075	1.4847
5.000	0.0245	0.0429	0.0919	0.3091	1.2046
10.000	0.0124	0.0220	0.0487	0.1815	0.8699

edge, so that the product $V_a \alpha T$ vanishes there. There are no further difficulties, since the integrand behaves like $1/\xi^2$ as $\xi \to \infty$.

It is natural to define starred functions for the special cases mentioned above; then 1) sinusoidal oscillations, $\alpha = \alpha_0 + \alpha_1 e^{i\omega t}$

$$I_w^* = C^*(k, X)$$
$$\alpha T = QC^* + i(2X - \tfrac{1}{2})\alpha_1 k e^{i\omega t}$$

2) indicial response to a step change in α

$$I_w^* = \Phi^*(s, X)$$
$$\alpha T = \Delta\alpha \Phi^*$$

3) sharp-edged gust response

$$I_w^* = \Psi^*(s, X)$$
$$\alpha T = w_0 \Psi^*$$

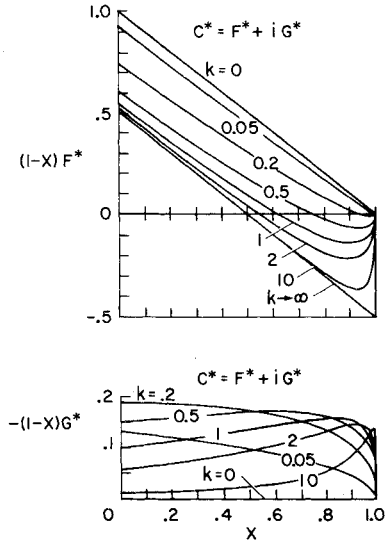

Fig. 2 Real and imaginary parts of the modified Theodorsen function for the velocity distribution on an oscillating airfoil.

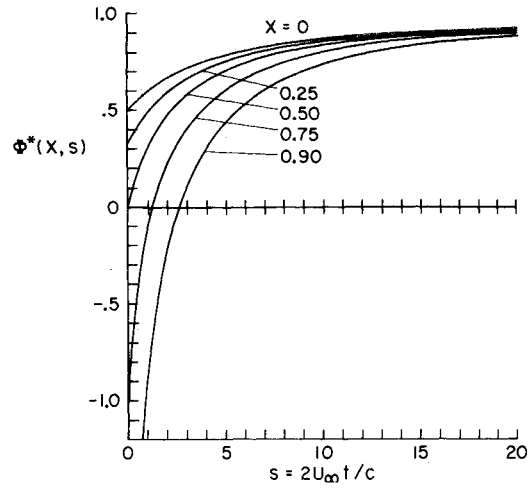

Fig. 3 Modified Wagner function for the velocity distribution on an airfoil with a step change in angle of attack.

The function $C^* = F^* + iG^*$ is plotted in Fig. 2 and tabulated in Table 1. The predominant behavior of $F^*(k, X)$ is given by

$$k \to 0; \quad F^* \approx F$$
$$k \gtrsim 1; \quad F^* \approx (F - X)/(1 - X)$$

The latter approximation improves with increasing k. The behavior of the function $G^*(k, X)$ is more complicated, and it changes in the vicinity of $k = 0.2$, where G attains its maximum negative value of -0.1886. Excluding the trailing edge region, G^* behaves approximately as follows:

$$k \to 0; \quad G^* \approx G[(1 - \tfrac{1}{2}X)/(1 - X)]$$
$$0.4 \lesssim k \lesssim 1; \quad G^* \approx [G + (G_{\max} - G)X]/(1 - X)$$
$$k \to \infty; \quad G^* \approx G/(1 - X)$$

The relationship between Φ^* and C^* is given by Eq. (A7) in the Appendix, and Fig. 3 shows the variation of Φ^* with X and s. The limiting behavior of Φ^* is the following:

$$s \to 0; \quad \Phi^* \approx (\Phi - X)/(1 - X)$$
$$s \to \infty \quad \Phi^* \approx \Phi$$

The results of this section are summarized in Table 2 for sinusoidal oscillations, $\alpha + \dot{h}/u_\infty = \alpha_0 + (\alpha_1 + h_1)\sin\omega t$. We see that the parameters of the unsteady motion are the reduced

Table 2 Summary of solutions for velocity, pressure, and stagnation point location on an oscillating airfoil

$$\alpha + \dot{h}/u_\infty = \alpha_0 + (\alpha_1 + h_1)\sin\omega t$$
$$U = V_t + V_c + V_a \alpha T$$
$$C_p = 1 - U^2 + 2V_a \alpha (T - R)$$
$$\tfrac{1}{2} C_{p\,\mathrm{LIN}} = 1 - V_t - V_c - V_a \alpha R$$
$$\left(\frac{dC_p}{dX}\right)_{\mathrm{LIN}} = -2\left(\frac{dV_t}{dX} + \frac{dV_c}{dX} + \frac{dV_a}{dX}\alpha S\right)$$
$$x_0 = \alpha^2 R^2(0, t)$$

where

$$\alpha T = \alpha_0 + \{h_1 F^* + \alpha_1[F^* - kG^*(\tfrac{3}{2} - 2A)]\}\sin\omega t + \{h_1 G^* + \alpha_1[G^* + kF^*(\tfrac{3}{2} - 2A) + 2k(X - \tfrac{1}{4})]\}\cos\omega t$$
$$\alpha R = \alpha_0 + \{h_1 F + \alpha_1[F - kG(\tfrac{3}{2} - 2A) + 2k^2 X(2A - X - \tfrac{1}{2})]\}\sin\omega t + \{h_1[G + 2kX] + \alpha_1[G + kF(\tfrac{3}{2} - 2A) + 2k(2X - \tfrac{1}{4})]\}\cos\omega t$$
$$\alpha S = \alpha_0 + \{h_1 F + \alpha_1[F - kG(\tfrac{3}{2} - 2A) - 4k^2 X(2X - 1)(X - A) + k^2 X]\}\sin\omega t + \{h_1[G + 2kX(2X - 1)] + \alpha_1[G + kF(\tfrac{3}{2} - 2A) + 4kX(2X - 1) - k/2]\}\cos\omega t$$

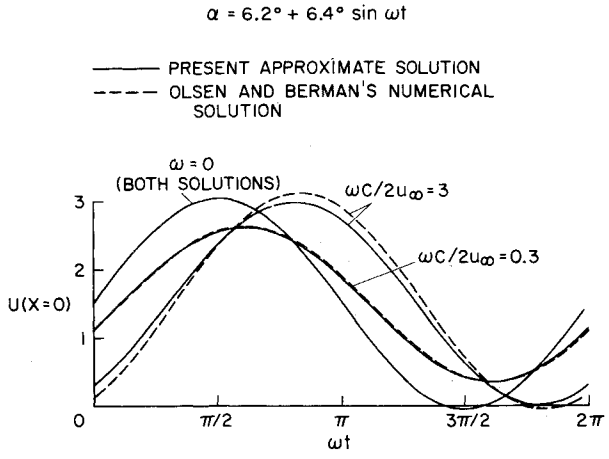

Fig. 4 Comparison of solutions for the leading edge velocity on an 11% symmetrical Joukowski airfoil pitching about $X = 0.5$.

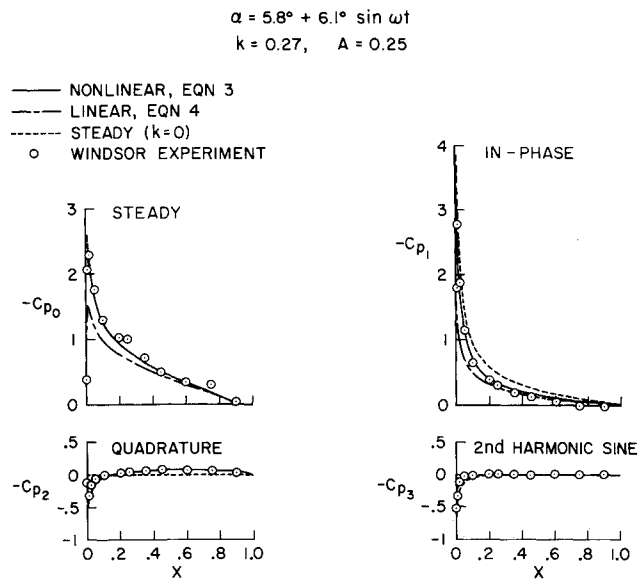

Fig. 6 Theoretical and experimental components of the upper surface pressure coefficient on an NACA 0012 airfoil pitching about $X = 0.25$. $C_p = C_{p0} + C_{p1} \sin \omega t + C_{p2} \cos \omega t + C_{p3} \sin 2\omega t + C_{p4} \cos 2\omega t$.

frequency k, the amplitude ratios α_1/α_0 and h_1/α_0, and the pitch axis location A. Airfoil thickness and camber effects enter through the functions V_t, V_c, and V_a, and leading-edge geometry would appear to be as important in the unsteady case as it is for stationary airfoils. Further physical insights will emerge in the following discussions.

Comparison with Numerical Solution

Figure 4 shows the results of the preceding section applied to the leading edge of an 11% thick symmetrical Joukowski airfoil, oscillating in pitch at $\alpha = 6.22° + 6.38° \sin \omega t$, for three values of reduced frequency. The quasi-steady ($k = 0$) velocity at $X = 0$ is linearly proportional to the instantaneous value of α. However, the phase lag and amplitude reduction grow rapidly with k, and significant unsteady effects are apparent even for $k = 0.3$.

Also shown in the figure are the recent numerical results of Olsen and Berman.[10] The excellent agreement between the two results at $k = 0.3$ is not surprising, since Allen's method[11] is accurate for the steady case and the actual wake deformation is small at this reduced frequency.

At the much larger k of 3.0, the agreement in the leading-edge velocities is still rather good, although one might wonder about the solution at other chordwise positions. Accordingly, the steady, in-phase, and quadrature components of U over the entire upper surface are plotted in Fig. 5. Not shown are the higher harmonics of velocity, which are zero in the present solution and very small in Olsen and Berman's results. The agreement is surprisingly good, except in the immediate vicinity of the trailing edge. This agreement is particularly gratifying in view of the simplicity and convenience of the present results.

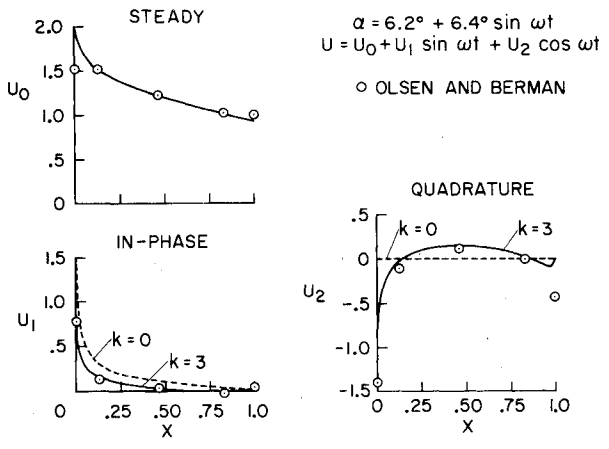

Fig. 5 Theoretical velocity components on the upper surface of an oscillating 11% symmetrical Joukowski airfoil; $A = 0.5$.

Comparison with Experiment

Figure 6 shows the various components of the absolute pressure coefficient on an oscillating NACA 0012 airfoil, in comparison with the highest frequency measurements of Windsor.[16] The solid line shows the values predicted by the nonlinear expression, Eq. (3), and the dashed line indicates the linearized values, Eq. (4). Both correctly predict the qualitative behavior of large phase lag and amplitude reduction near the leading edge, but for quantitative agreement one must sacrifice the simplicity of the linearized result for the accuracy of the complete Bernouilli equation when dealing with the pressure.

Finally, we should observe that the linearized result does not admit second harmonics. However, the data show small but finite values of C_{p3} and C_{p4} in the important region near the leading edge, and these are well-represented by the complete pressure formula, Eq. (3).

III. Consideration of Separation and Stall

The general problem of airfoil stall remains unsolved, although the basic features have been categorized for the steady case and the angle of attack for static stall α_{ss} is well-documented for many profiles.[12,17] It is also well-known that oscillating airfoils exhibit complex stall hysteresis. That is, an airfoil with positive $\dot{\alpha}$ stalls at an angle α_{DS} greater than the static stall angle, α_{ss}, while the stall recovery during negative $\dot{\alpha}$ occurs at an angle less than α_{ss}. And, as the airfoil oscillates in and out of stall, the dynamic forces and moments can attain values that are far greater than their static counterparts.

Since viscous effects are involved, the problem of stall and reattachment prediction would seem to lie beyond the scope of this investigation. However, Carta[18] recently speculated that the phase lag and attenuation of the inviscid pressure distribution could significantly delay the onset of dynamic stall to angles of attack well beyond α_{ss}. Since Patey's results[19] and unpublished boundary-layer calculations of the writer have indicated that laminar skin friction and separation are hardly affected by unsteady viscous effects for many of the unsteady airfoil cases of

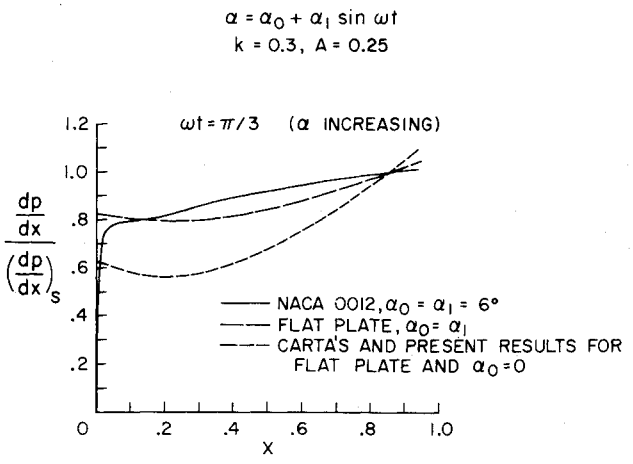

Fig. 7 Examples of the reduction in the chordwise pressure gradients on pitching airfoils when $\dot{\alpha} > 0$.

practical interest, Carta's proposal of unsteady inviscid effects would seem to have some merit.

Carta's analysis was restricted to a flat plate with $\alpha_0 = 0$, but the results of Sec. II now permit us to examine more carefully the pressure gradients in the important leading edge region of an airfoil with thickness. The X-derivative of Eq. (4) can be written as

$$(dC_p/dX)_{\text{LIN}} = -2[dV_t/dX + dV_c/dX + (dV_a/dX)\alpha S] \quad (12)$$

where $S(X,t)$ is given in Table 2. Directly analogous to R and T in Sec. II, the function S is the ratio of the unsteady to quasi-steady pressure gradients on a flat plate.

Figure 7 shows flat plate and airfoil results for $\alpha_0 = 6°$ superimposed on Carta's Fig. 3. A reduction in adverse pressure gradients due to unsteady effects is evident in all cases, but the magnitude of the effect is different when airfoil thickness and mean angle of attack are included.

Now Carta's basic premise is that the chordwise adverse pressure gradient on the airfoil is one of the most crucial factors in determining the stall angle of attack. Pursuing this idea more specifically, let us postulate that some boundary-layer separation event occurs when dC_p/dX near the leading edge attains a certain value, whatever the rate of change of α. Assuming that we know this critical value and the angle at which it occurs in the steady case, α_{static}, then the assumption is that the same viscous event will occur in the dynamic case, $\alpha = \alpha_0 + \alpha_1 \sin \omega t$, at the same value of dC_p/dX but a different angle of attack, α_{dynamic}. Therefore, we can set Eq. (12) equal to $(dC_p/dX)_{\text{static}}$ and solve for α_{dynamic}, giving the dynamic overshoot

$$\frac{\alpha_{\text{dynamic}} - \alpha_{\text{static}}}{\alpha_1} = \frac{g}{(f^2+g^2)^{1/2}} + \left(\frac{\alpha_{\text{static}} - \alpha_0}{\alpha_1}\right)\left[\frac{1}{(f^2+g^2)^{1/2}} - 1\right] \quad (13)$$

where f and g are the in-phase and quadrature components of S (cf, Table 2),

$$f = F - kG(\tfrac{3}{2} - 2A) - 4k^2X[(2X-1)(X-A) - \tfrac{1}{4}]$$
$$g = -G - kF(\tfrac{3}{2} - 2A) - 2k[2X(2X-1) - \tfrac{1}{4}]$$

It should be mentioned that since f and g depend upon X as well as A and k, the theoretical separation or stall angles will depend somewhat upon the choice of X where the critical event is assumed to occur, e.g., leading-edge stall, trailing edge separation, separation bubble, etc. Also, if the airfoil oscillates in and out of stall, the viscous-inviscid interaction may in some cases alter the vorticity distribution in the wake enough to affect the inviscid solution throughout the cycle, even during the time below the stall angle.

Another interesting result has been suggested by J. H. Olsen in a private communication[26]; namely, under certain conditions the angle of attack can briefly exceed α_{static} without $(dC_p/dX)_{\text{dynamic}}$ ever attaining the critical static value. To satisfy this condition that the dynamic pressure gradient at an arbitrary point X must always be less than the corresponding static gradient, we find from Eq. (12) that the amplitude of the oscillation must be

$$\alpha_1 < [(\alpha_{\text{static}} - \alpha_0)/(f^2+g^2)^{1/2}] \quad (14)$$

Now in general, $(f^2+g^2)^{1/2} < 1$ for $k > 0$. Since $\alpha = \alpha_0 + \alpha_1 \sin \omega t$, it is possible that at the top of the cycle α can exceed α_{static} without precipitating the viscous event in question, at least within the framework of our basic hypothesis. This is different from the situation described by Eq. (13), wherein the viscous event does occur, but at a later time. The significance of Eq. (14) is that it can be used to define a theoretical stall-free regime above the static stall angle, where presumably we should still be able to apply potential flow and thin boundary-layer theory with confidence.

A Simple Experiment

To assess the validity of the preceding hypotheses about the differences between static and dynamic airfoils, an oscillating NACA 0012 model was tested under the following conditions: $0 \leqq k \leqq 0.5$, $6° \leqq \alpha_0 \leqq 13°$, $4° \leqq \alpha_1 \leqq 19°$, $A = 0.25$, and $Re = 3.5 \times 10^5$ and 5×10^5. The chord and span of the model were 15.2 and 30.5 cm, respectively. The instrumentation consisted of a heated-film skin-friction gage[20] and a small fast-response pressure transducer at $X = 0.1$, and hot-wire anemometers at $X = 0.1$, 0.25, and 0.75.

The hot wires were normally mounted just outside the boundary layer and used to detect large-scale disturbances in the inviscid flow that might be symptomatic of stall. The hot wire at $X = 0.1$ was also moved into the boundary layer, where it and the skin-friction gage provided transition and separation data. Oil flow visualization at $k = 0$ provided additional information to support the interpretation of the hot wire and skin-friction signals.

The experiment produced three distinct types of results. The first, which could be compared directly with Eq. (13), was a local boundary-layer separation and reattachment that occured below the stall angle and did not significantly affect the potential flow around the airfoil or the trailing vorticity in the wake. This laminar separation bubble moved forward over the airfoil as α increased and was easily detected by the skin-friction gage. Another type of result was obtained by oscillating the airfoil so that the maximum incidence exceeded the static stall angle by only a few degrees and observing whether stall occurred at any time during the cycle. By varying the frequency over a wide range, an experimental stall boundary that could be compared with Eq. (14) was generated. Finally, the airfoil was oscillated about the static stall angle, and the incidence for the onset of dynamic stall was observed. These more conventional results were compared with data from other sources[16,21-23] and with Eq. (13).

It should be mentioned that despite considerable difference in their signals after stall began, all five transducers registered the initial onset of stall virtually simultaneously in almost every case. Such behavior would generally be associated with the so-called leading-edge type of stall for steady airfoils.

Results for Laminar Separation

Figure 8 shows the measured and predicted variation in the angle of attack for laminar separation at the gage location $X = 0.1$, as a function of reduced frequency; the ordinate in Fig. 8 is merely a convenient rearrangement of Eq. (13). It should be mentioned that in the case of $\alpha_1 = 19°$, stall occurred during the later portion of the cycle. However, the large values of $\dot{\alpha}$ at the α_{static} for this discussion (approximately 7°) apparently dominated the laminar separation at $X = 0.1$, and the results agree with the completely unstalled data for $\alpha_1 = 6.2°$.

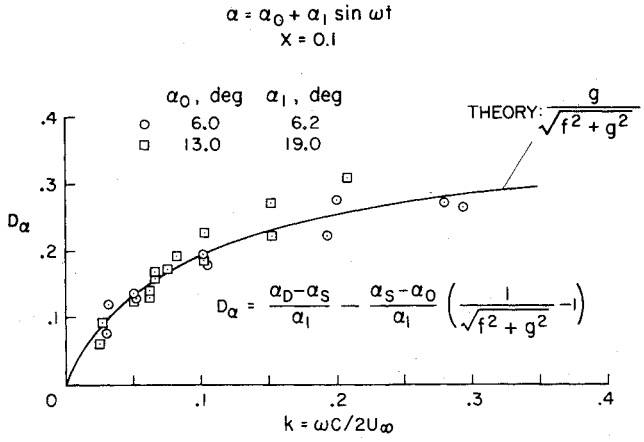

Fig. 8 Comparison of the theoretical and experimental dynamic delay in laminar separation on an NACA 0012 airfoil; α_S and α_D denote the static and dynamic angles of attack, respectively, for laminar separation at $X = 0.1$.

The excellent agreement between the inviscid theory and the data verifies Carta's basic idea for this particular viscous phenomenon, and indicates that the important unsteady effects occur in the potential flow, rather than in the boundary layer itself.

Results for Dynamic Stall

The first case to be considered is the extent to which the static stall angle can be exceeded without dynamic stall occurring anywhere in the cycle. The upper limits predicted by Eq. (14), evaluated at several chordwise stations, are shown in Fig. 9. Also shown are the experimental conditions for which stall was and was not observed. The half-solid symbols denote several test points for which stall was observed during some cycles and not during others, or for which only one or two transducers showed evidence of stall. These points assisted in determining the experimental stall boundary.

The measured boundary can be seen to rise with increasing frequency; however, the quantitative agreement with theory is much less satisfactory than in Fig. 8. In this case, the measured stall delay is significantly less than predicted.

By contrast, the measured increase in the angle of attack for the onset of dynamic stall for airfoils oscillating in and out of

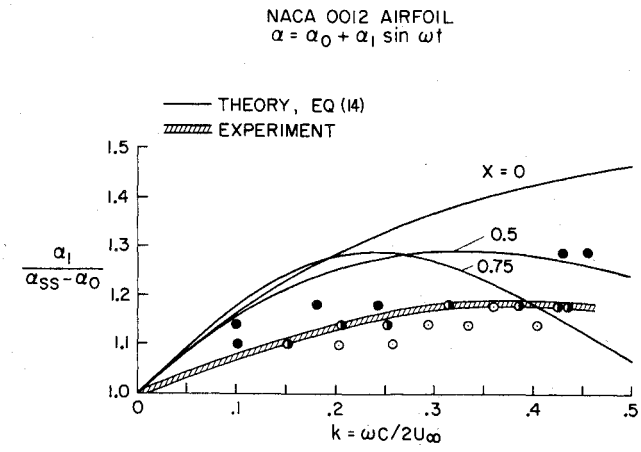

Fig. 9 Theoretical and experimental boundaries for exceeding the static stall angle with no evidence of stall. Open symbols denote absence of stall throughout the cycle; solid symbols denote complete stall during some part of the cycle.

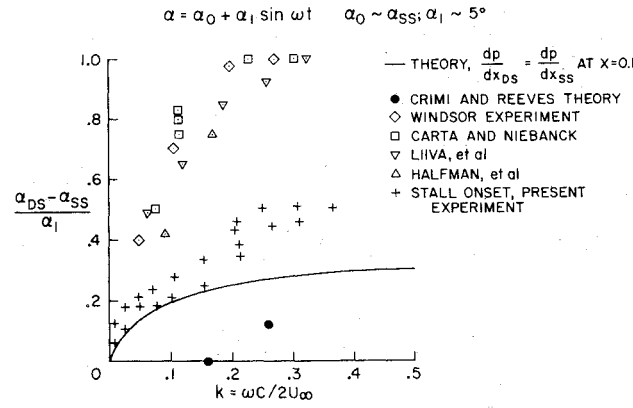

Fig. 10 Theoretical and experimental stall delay on oscillating NACA 0012 airfoils. Open symbols denote moment stall data; + denotes initial breakdown of the potential flow.

stall, shown in Fig. 10, is significantly greater than predicted by Eq. (13). In this figure, $\alpha_0 \approx \alpha_{ss}$, $4.5° < \alpha_1 < 6.2$, and the present data correspond to the angle of attack where the inviscid flowfield first began to break down, somewhat in advance of complete stall. The theory of Crimi and Reeves[9] and the data of other investigation[16,21-23] correspond to the angles of attack where nose-down pitching moments increased abruptly, usually the first large-scale manifestation of dynamic stall.[24] The spread between the two types of data can be attributed to the finite time span required for dynamic stall to develop; in fact, the maximum lift was attained even later. But the point here is that no indication of stall whatsoever appears until the airfoil has moved well past the theoretical predictions.

The obvious conclusion to be drawn from the poor quantitative agreement between theory and experiment in Figs. 9 and 10 is that, unlike the laminar separation results described previously, some sort of unsteady viscous effects must be influencing the actual dynamic stall delay, and the purely inviscid pressure gradient criterion will not suffice for predicting the major differences between static and dynamic stall. In addition, the data indicate that the dynamic stall process does not occur instantaneously, but requires a finite period of time between the first major disturbances in the potential flow and the final flow breakdown that causes an abrupt loss in lift. Perhaps the analysis of the previous section could be coupled with unsteady boundary-layer theory or extended to incorporate viscous interaction, but we are forced to conclude that not even the delay in the very onset of dynamic stall can be predicted from purely inviscid considerations.

IV. Summary and Conclusions

The analysis presented in this paper consists of three straightforward steps: 1) the boundary condition on the airfoil and in the wake is linearized, permitting the velocity potential to be separated into thickness, camber, and angle-of-attack components; 2) Allen's method for steady airfoils is employed to improve the accuracy of the solution; and 3) Theodorsen's analysis of an unsteady flat plate is used to describe the effects of the unsteady wake. This enables a complete and accurate solution to be developed with no new elaborate mathematical analysis. Furthermore, the results are simple enough to permit the predominant aerodynamic and geometric parameters to be seen explicitly, given the steady solution of the airfoil.

Going beyond the normal limits of an inviscid investigation, explanations of certain viscous phenomena were pursued using purely inviscid notions about the longitudinal pressure gradients on the airfoil. The combined theoretical and experimental results of this pursuit indicate that unsteady viscous effects on oscillating airfoils are much less important than unsteady potential flow

effects, if the boundary layer does not interact significantly with the main flow. However, this does hold true in the important viscous inviscid interaction problem known as dynamic stall. In this case, the inviscid theory correctly indicates the trends in the onset of large scale boundary-layer separation, but not the quantitative delay above the angle of attack for static stall. As far as the practical manifestations of dynamic stall are concerned, the inviscid criterion grossly underestimates the angles of attack where pitching moment and lift first exhibit stall behavior. Therefore, there appears to be a great deal left to be done in solving the important problem of dynamic stall.

Appendix

In treating the oscillating flat plate in a uniform stream, Theodorsen[1] splits the velocity potential into noncirculatory components, which depend solely upon the instantaneous motion of the airfoil, and the circulatory components due to the time-dependent sheet of vorticity in the wake. The strength of this sheet is adjusted to satisfy the Kutta condition of finite velocities at the trailing edge at each instant.

If we apply the mean surface approximation to an airfoil with thickness and camber, the flat plate solution becomes the unsteady counterpart of the "additional lift distribution," V_a, in Allen's theory,[11] and the thickness and camber components of U are independent of time for a rigid airfoil. Since V_t and V_c do not alter the Kutta condition or the trailing edge matching condition of the circulatory and noncirculatory components of V_a, the calculation of the unsteady wake depends only upon the airfoil motion and is independent of the airfoil geometry.

In the semichord notation $x = (2X - 1)$, Theodorsen gives the following expressions for the components of ϕ_a and for the Kutta condition:

$$\phi_{\text{noncirculatory}} = \left[\alpha + \frac{\dot{h}}{u_\infty} + \frac{\dot{\alpha}c}{2u_\infty}\left(\frac{x}{2} - a\right)\right](1-x^2)^{1/2} \tag{A1}$$

$$\left(\frac{\partial\phi}{\partial x}\right)_{\text{circulatory}} = \frac{\Gamma_0}{2\pi(1-x^2)^{1/2}}\int_1^\infty \frac{(\xi^2-1)^{1/2}\,e^{-ik\xi}\,d\xi}{(\xi - x)} \tag{A2}$$

$$\left(\frac{\partial\phi}{\partial t}\right)_{\text{circulatory}} = \frac{u_\infty \Gamma_0 (1-x^2)^{1/2}}{2\pi c}\int_1^\infty \frac{e^{-ik\xi}\,d\xi}{(\xi^2-1)^{1/2}(\xi - x)} \tag{A3}$$

$$\frac{\Gamma_0}{2\pi}\int_1^\infty \left(\frac{\xi+1}{\xi-1}\right)^{1/2} e^{-ik\xi}\,d\xi = u_\infty \alpha + \dot{h} + \left(\frac{1}{2} - a\right)\frac{\dot{\alpha}c}{2} \tag{A4}$$

If we are only interested in the pressure distribution, the linearized expression for the circulatory components in the *sum* of Eqs. (A2) and (A3), which is

$$(C_p)_{\text{circulatory}} = \frac{-\Gamma_0}{\pi(1-x^2)^{1/2}}\int_1^\infty \frac{(\xi + x)}{(\xi^2-1)^{1/2}}\,e^{-ik\xi}\,d\xi = \frac{\Gamma_0}{2(1-x^2)^{1/2}}\left[J_1 + xY_0 - i(Y_1 - xJ_0)\right] \tag{A5}$$

That is, the effect of the wake on the pressure can be expressed in terms of the Bessel functions, $J_n(k)$ and $Y_n(k)$. The use of Eq. (A4) to evaluate Γ_0 and further algebraic manipulations lead to Eq. (8).

Unfortunately, neither Eq. (A2) nor (A3) alone can be reduced to combinations of Bessel functions or other standard integrals. Therefore, we are forced to evaluate numerically one or other of the integrals; the one in Eq. (A3) is easier because of the behavior of the integrand at large ξ. This integration, facilitated by the change of variable $\xi = \cosh\eta$, provides the values of C^* given in Table 1 and Fig. 2. The complete solution using C and C^* is summarized in Table 2.

The wake integral I_w^* for velocity for other airfoil motions can be developed in the same way, merely substituting $\gamma_w(\xi, t)$ for $\Gamma_0 e^{-ik\xi}$ in the preceding equations. A particularly interesting case is the step change in α; in this case, Garrick[25] shows that the Wagner function is related to the Theodorsen function as follows:

$$\Phi(s) = \frac{2}{\pi}\int_0^\infty \frac{F(k)\sin ks\,dk}{k} \tag{A6}$$

Similarly

$$\Phi^*(s, X) = \frac{2}{\pi}\int_0^\infty \frac{F^*(k, X)\sin ks\,dk}{k} \tag{A7}$$

Figure 3 shows the result of this integration.

References

[1] Theodorsen, T., "General Theory of Aerodynamic Instability and the Mechanism of Flutter," Rept. 496, 1935, NACA.

[2] Wagner, H., "Über die Entstehung des dynamischen Auftriebs von Traflugeln," *Zeitschrift für Angewandte Mathematik und Mechanik*, Vol. 5, No. 1, Jan. 1925, pp. 17–35.

[3] Kussner, H. G., "Zusammenfassender Bericht über den instationaren Auftrieb von Traflugeln," *Luftfahrtforschung*, Vol. 13, No. 12, Dec. 1936, pp. 410–424.

[4] von Kármán, T. and Sears, W. R., "Airfoil Theory for Non-Uniform Motion," *Journal of the Aeronautical Sciences*, Vol. 5, No. 10, Aug. 1938, pp. 379–390.

[5] Kussner, H. G., "Non-Stationary Theory of Airfoils of Finite Thickness in Incompressible Flow," *AGARD Manual on Aeroelasticity*, Vol. II, Oct. 1968, Chap. 8.

[6] Woods, L. C., "The Lift and Moment on a Thick Aerofoil in Unsteady Motion," *Philosophical Transactions of the Royal Society*, Vol. A247, No. 11, Nov. 1954, pp. 131–162.

[7] Chen, C. F. and Wirtz, R. A., "Second Order Theory for Flow Past Oscillating Foils," TR 116-ME-F, Aug. 1967, Dept. of Mechanical and Aerospace Engineering, Rutgers Univ., New Brunswick, N.J.

[8] Giesing, J. P., "Nonlinear Two-Dimensional Unsteady Potential Flow with Lift," *Journal of Aircraft*, Vol. 5, No. 2, March-April 1968, pp. 135–143.

[9] Crimi, P. and Reeves, B. L., "A Method for Analyzing Dynamic Stall," AIAA Paper 72-37, San Diego, Calif., 1972.

[10] Olsen, J. H. and Berman, C. H., "Potential Flow about Pitching Joukowski Airfoils," D210-10406-1, Dec. 1971, Boeing Scientific Research Lab., Seattle, Wash.

[11] Allen, H. J., "A Simplified Method for the Calculation of Airfoil Pressure Distribution," TN 708, 1939, NACA.

[12] Abbott, I. H. and von Doenhoff, A. E., *Theory of Wing Sections*, Dover, New York, 1959; also Rept. 824, 1945, NACA.

[13] van Dyke, M. D., "Second Order Subsonic Airfoil Theory Including Edge Effects," Rept. 1274, March 1956, NACA.

[14] Ville, G., "Influence des Décollements au Bord d'Attaque sur les Caractéristiques Aérodynamiques des Voilures," *4th Colloque d'Aérodynamique Appliquée*, Association Francaise des Ingénieurs et Techniciens de l'Aéronautique et de l'Espace, Lille, Nov. 1967; also TTF-12, 546, 1969, NASA.

[15] Bisplinghoff, R. L., Ashley, H., and Halfman, R. L., *Aeroelasticity*, Addison-Wesley, Reading, Mass., 1957, pp. 251–293.

[16] Windsor, R. I., "Measurement of Aerodynamic Forces on an Oscillating Airfoil," TR 69-98, March 1970, U.S. Army Aviation Material Lab., Ft. Eustis, Va.

[17] van den Berg, B., "Reynolds Number and Mach Number Effects on the Maximum Lift and the Stalling Characteristics of Wings at Low Speeds," TR 69025U, 1969, National Aerospace Lab. NLR, Amsterdam.

[18] Carta, F. O., "A Theoretical Study of the Effect of Unsteady Pressure Gradient on Dynamic Stall Delay," *Journal of Aircraft*, Vol. 8, No. 10, Oct. 1971, pp. 839–841.

[19] Patey, S. A., "Leading Edge Separation on an Airfoil during Dynamic Stall," Aeronautics and Structures Report ASRL TR 156-1, Oct. 1969, MIT, Cambridge, Mass.

[20] McCroskey, W. J. and Durbin, E. J., "Flow Angle and Shear Stress Measurements Using Heated Films and Wires," *Transactions of the ASME, Ser. D; Journal of Basic Engineering*, Vol. 94, No. 1, March 1972, pp. 46–52.

[21] Liiva, J. and Davenport, F. J., "Two-Dimensional Tests of Airfoils Oscillating near Stall," TR 68-13, 1968, U.S. Army Aviation Material Lab., Ft. Eustis, Va.

[22] Carta, F. O. and Niebanck, C. F., "Prediction of Rotor Instability at High Forward Speeds, Vol. 3, Stall Flutter," TR 68-18C, 1969, U.S. Army Aviation Material Lab., Ft. Eustis, Va.

[23] Halfman, R. F., Johnson, H. C., and Haley, S. M., "Evaluation of High Angle-of-Attack Aerodynamic-Derivative Data and Stall-Flutter Prediction Techniques," TN 2533, Nov. 1951, NACA.

[24] Harris, F. D. and Pruyn, R. R., "Blade Stall. Half Fact, Half Fiction," *Journal of the American Helicopter Society*, Vol. 13, No. 2, April 1968, pp. 27–48.
[25] Garrick, I. E., "On Some Fourier Transforms in the Theory of Non-Stationary Flows," *Proceedings of the Fifth International Congress on Applied Mechanics*, Wiley, New York, 1938, pp. 590–593.
[26] Olsen, J. H., private communication, Nov. 1971, Flow Research Corp., Kent, Wash.

AUGUST 1973 AIAA JOURNAL VOL. 11, NO. 8

Hypersonic Wake Aerodynamics at High Reynolds Numbers

MICHAEL L. FINSON*
Avco Everett Research Laboratory Inc., Everett, Mass.

Motivated by ballistic range shadowgraphs, a theory has been developed for the wakes of slender cones under hypersonic, turbulent boundary-layer conditions. In the proposed model, the near wake is dominated by residual boundary-layer turbulence. It is shown that the intensity and scale size of this turbulence should be considerably smaller than equilibrium wake turbulence values. The resulting low-eddy viscosity provides an explanation for the slow observed wake growth. An approximate method is formulated for computing the near wake development of the turbulent intensities, Reynolds stress, and macroscale. Calculations in the expansion region suggest that a necessary condition for the postulated dominance of the near wake by residual boundary-layer turbulence is that the Reynolds number be sufficiently large that the boundary-layer turbulence not "relaminarize" upon expansion. The eventual recovery to equilibrium wake turbulence is predicted to require downstream distances of many hundreds of body diameters. Computed wake growth rates compare favorably with shadowgraph data.

I. Introduction

AT moderate Reynolds numbers, the boundary layer on a body moving at hypersonic speeds is laminar and transition to turbulence occurs in the wake. Some time ago Lees and Hromas[1] showed that, downstream of the transition zone, the wake grows in a manner which may be described well by calculations based on a locally similar turbulent mixing rate. Recent ballistic range shadowgraphs have suggested a very different wake behavior at higher Reynolds numbers, where there is a well-developed turbulent boundary layer on the body. As an example, Fig. 1 shows shadowgraphs of the near wakes of two cone launchings carried out at the Naval Ordnance Lab.[2] For the case shown in the upper photograph, at $M_\infty = 6.3$, the boundary layer is laminar. Due to the relatively high Reynolds number in this laminar case ($Re_{\infty,D} = 3 \times 10^6$), there is no noticeable laminar run in the wake. Transition occurs in the neck region, and seems to cause a rapid establishment of large scaled, intense wake turbulence. In the lower photograph the boundary layer is clearly turbulent. Although it must be recognized that shadowgraphs can provide distorted impressions of the flow (they respond to the second derivative of the density, and may observe only the outer portions of the wake), there appears to be a distinct difference in flow structure between the two cases. This difference was first noticed by Levensteins and Krumins[3] in their analysis of these and many other shadowgraphs. Both the standard deviation and the correlation microscale of the wake edge location were found to be significantly smaller in the turbulent boundary-layer case. They noted that "It appears that the scale of turbulence that exists in the turbulent boundary layer persists for some distance downstream in the wake. Subsequently, a transition to larger-scale turbulence occurs. For the flow

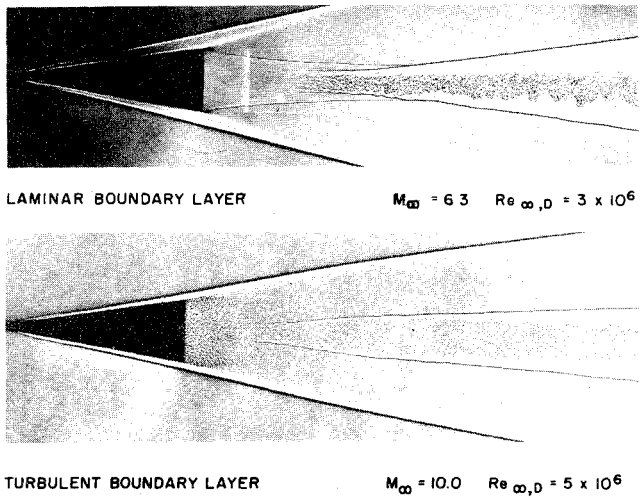

Fig. 1 Naval Ordnance Lab. ballistic range shadowgraphs[2] of typical laminar and turbulent boundary-layer cases.

Presented as Paper 72-701 at the AIAA 5th Fluid and Plasma Dynamics Conference, Boston, Mass., June 26–28, 1972; submitted September 1, 1972; revision received February 26, 1973. This work was supported by the U.S. Army, Advanced Ballistic Missile Defense Agency, under contract DAHC 60-69-C-0013.
Index categories: Jets, Wakes, and Viscid-Inviscid Flow Interactions; Supersonic and Hypersonic Flow; Viscous Nonboundary Layer Flows.
* Principal Research Scientist. Member AIAA.